Distribution System Restoration with Cyber Failures Based on Co-dispatching of Multiple Recovery Resources

Zhengze Wei, Kaigui Xie, Bo Hu, Yu Wang, Changzheng Shao, Pierluigi Siano, and Jun Zhong

***Abstract*—Improving the restoration efficiency of a distribution system is essential to enhance the ability of power systems to deal with extreme events. The distribution system restoration (DSR) depends on the interaction among the electric network (EN), cyber network (CN), and traffic network (TN). However, the coordination of these three networks and co-dispatching of multiple recovery resources have been mostly neglected. This paper proposes a novel DSR framework, which is formulated as a mixed-integer linear programming (MILP) problem. The failures in cyber lines result in cyber blind areas, which restrict the normal operation of remote-controlled switches. To accelerate the recovery process, multiple recovery resources are utilized including electric maintenance crews (EMCs), cyber maintenance crews (CMCs), and emergency communication vehicles (ECVs). Specifically, CMCs and ECVs restore the cyber function of switches in cooperation, and EMCs repair damaged electric lines. The travel time of these three dispatchable resources is determined by TN. The effectiveness and superiority of the proposed framework are verified on the modified IEEE 33-node and 123-node test systems.**

***Index Terms*—Distribution system restoration (DSR), network coupling, maintenance crew, co-dispatching, emergency communication vehicle.**

NOMENCLATURE

A. Sets and Indices

$\kappa \in \{emc, cmc, ecv\}$	Set of indices for three dispatchable resources, i.e., electric maintenance crew (EMC), cyber maintenance crew (CMC), and emergency communication vehicle (ECV)
$O(\kappa)$	Index for starting vertices of dispatchable resource κ
$D(\kappa)$	Index for ending vertices of dispatchable resource κ
a, b	Indices for electric (cyber) node blocks
B	Set of electric (cyber) node blocks
B^{sub}	Set of substation node blocks
c	Index for cyber blind areas
C	Set of cyber blind areas
d	Index for depots
$d(emc)$, $d(cmc)$	Indices for the depots, where *emc* and *cmc* depart and return, respectively
$d(ecv)$	Index for the depot, where *ecv* departs and returns
$d(m)$	Index for depot assigned to repair task at vertex m
$ds(i)$	Set of downstream nodes connected to node i
D	Set of depots
emc, cmc	Indices for EMC and CMC
ecv	Index for ECV
e, f	Indices for vertices V_{ecv}^{EN} in electric network (EN) graph
i, j	Indices for electric (cyber) nodes
l	Index for electric (cyber) lines
L_a^{EMC}	Set of damaged lines in electric (cyber) node block a
m, n	Indices for vertices V_{emc}^{EN} in EN graph
N_c	Set of cyber nodes in cyber blind area c
N, L	Sets of electric (cyber) nodes and lines
N_a, L_a	Sets of nodes and lines in electric (cyber) node block a
N_{T}, L_{T}	Sets of traffic nodes and lines
p, q	Indices for vertices V^{CN} in cyber network (CN) graph
T^{R}	Set of energization time t_i^{R}

Manuscript received: March 18, 2023; revised: July 3, 2023; accepted: September 18, 2023. Date of CrossCheck: September 18, 2023. Date of online publication: December 6, 2023.

This work was supported by the National Natural Science Foundation of China (No. 52007016).

Z. Wei, K. Xie (corresponding author), B. Hu, Y. Wang, and C. Shao are with the National Key Laboratory of Power Transmission Equipment Technology, Chongqing University, Chongqing 400044, China (e-mail: zhengze_wei@163.com; kaiguixie@vip.163.com; hboy8361@163.com; yu_wang@cqu.edu.cn; cshao@cqu.edu.cn).

P. Siano is with the Department of Management and Innovation Systems, University of Salerno, Fisciano 84084, Italy, and he is also with the Department of Electrical and Electronic Engineering Science, University of Johannesburg, Johannesburg 2006, South Africa (e-mail: siano.pierluigi@gmail.com).

J. Zhong is with the Shenzhen Power Supply Co., Ltd., China Southern Power Grid, Shenzhen 518000, China (e-mail: zhongjuncqu@gmail.com).

DOI: 10.35833/MPCE.2023.000173

$us(i)$ Set of upstream nodes connected to node i

V^{EN} Set of EMC and ECV depots, damaged electric lines, and remote-controlled switches

V^{CN} Set of CMC depots and damaged cyber lines

V^{CN}_{cmc} Set of CMC depots and damaged cyber lines in CN

V^{DCL} Set of damaged cyber lines

V^{EN}_{emc} Set of EMC depots and damaged electric lines in EN

V^{EN}_{ecv} Set of ECV depots and remote-controlled switches in EN

V^{RS} Set of remote-controlled switches

$V^{\mathrm{RS}}_{\mathrm{int}}$ Set of remote-controlled switches with intact cyber function

B. Parameters

ω_i Priority and weight of load at node i

$h_{ij}(t)$ Capacity of road ij at time t

$l_{d,m}$ The shortest path distance from damaged electric line at vertex m to depot d

l_{ij} Distance between traffic nodes i and j

$h^{\max}_{ij}$ The maximum capacity limit of road ij

M, ζ Large (or small) numbers for modeling and linearization

$P^{\mathrm{load}}_i, Q^{\mathrm{load}}_i$ Active and reactive load demands at electric node i

$P^{\mathrm{G,max}}_i$, $Q^{\mathrm{G,max}}_i$ The maximum generation limits of active and reactive power at electric node i

$P^{\max}_{i,j}, Q^{\max}_{i,j}$ The maximum limits of active and reactive power of electric line ij

$R_{i,j}, X_{i,j}$ Resistance and reactance of electric line ij

r, s, δ Coefficients of different road types

$T^{\mathrm{rep}}_{m,emc}$ Time required for emc to repair damaged electric line at vertex m

$T^{\mathrm{rep}}_{p,cmc}$ Time required for cmc to repair damaged cyber line at vertex p

T^{op}_{ecv} Operation time after ecv arrives at destination

$T^{\mathrm{RS}}_{a,b}$ Time required to close remote-controlled switch between electric nodes a and b

$T^{\mathrm{tr}}_{m,n,emc}$ Time required for emc to travel from vertices m to n

$T^{\mathrm{tr}}_{e,f,ecv}$ Time required for ecv to travel from vertices e to f

$T^{\mathrm{tr}}_{p,q,cmc}$ Time required for cmc to travel from vertices p to q

$U^{\max}_i, U^{\min}_i$ The maximum and minimum voltage limits of electric node i

U_0 Reference voltage

$v_{ij}(t)$ Travel speed between traffic nodes i and j at time t

$v_{ij,0}$ Zero-flow speed of road ij

C. Decision Variables

$P_{i,j,t}, Q_{i,j,t}$ Active and reactive power of electric line ij at time t

$P^{\mathrm{G}}_{i,t}, Q^{\mathrm{G}}_{i,t}$ Active and reactive power generations of electric node i at time t

$t^{\mathrm{comp}}_m, t^{\mathrm{comp}}_p$ Repair completion time for damaged electric (cyber) line at vertices m and p

t^{CR}_i Time for cyber function of cyber node i to be restored

t^{DSRM}_a Energization time of electric node block a

$t^{\mathrm{reach}}_{m,emc}, t^{\mathrm{reach}}_{p,cmc}$ Time when emc and cmc reach damaged electric (cyber) line or depot at vertices m and p

$t^{\mathrm{reach}}_{e,ecv}, t^{\mathrm{leave}}_{e,ecv}$ Time when ecv reaches and leaves remote-controlled switch or depot at vertex e

t^{R}_i Energization time of electric node i

$t^{\mathrm{RS}}_{a,b}$ Closing completion time of remote-controlled switch connecting electric node blocks a and b

$T^{\mathrm{stay}}_{e,ecv}$ Time for ecv to stay at vertex e

u^{ECV}_{rs} Binary variable indicating whether cyber function of remote-controlled switch rs is temporarily restored by ECV

u^{CMC}_{rs} Binary variable indicating whether cyber function of remote-controlled switch rs is temporarily restored by CMCs

$U_{i,t}$ Voltage of electric node i at time t

$z^{\mathrm{DSRM}}_{a,b}$ Binary variable indicating whether remote-controlled switch between electric node blocks a and b is closed with energization direction from a to b

$z^{\mathrm{ES}}_{a,b,t}$ Binary variable indicating energization status of remote-controlled switch ab at time t

$z^{\mathrm{FAM}}_{d,m}$ Binary variable indicating whether damaged electric line vertex m is allocated to depot d

$z^{\mathrm{FAM}}_{d,p}$ Binary variable indicating whether damaged cyber line vertex p is allocated to depot d

$z_{e,f,ecv}$ Binary variable indicating whether ecv travels from vertices e to f

$z^{\mathrm{ES}}_{i,t}$ Binary variable indicating energization status of electric node i at time t

$z^{\mathrm{ES}}_{i,j,t}$ Binary variable indicating energization status of electric line ij at time t

$z_{m,n,emc}$ Binary variable indicating whether an emc travels from vertices m to n

$z_{p,q,cmc}$ Binary variable indicating whether cmc travels from vertices p to q for repair work

I. Introduction

MODERN distribution systems are highly coupled power supply systems that include electric networks (ENs) and cyber networks (CNs), and have a high degree of

automation and strong self-healing ability. In recent years, extreme events such as typhoons, ice storms, rainstorms, and cyberattacks have become increasingly frequent [1], posing significant threats to ENs and CNs. The coupling and dependency between ENs and CNs have seriously affected the recovery process and reduced the ability and efficiency of rapid load restoration in distribution systems [2]. For example, in 2012, Hurricane "Sandy" seriously damaged the ENs and CNs of New York in the United States. In addition, a large-scale interruption of communications led to delays in failure reparation works. Over 170 thousand consumers did not have power supply for half a month after this disaster [3]. Hence, the collaborative restoration of ENs and CNs is essential for distribution systems to suitably cope with extreme events.

Conventional distribution system restoration (DSR) focuses on power supply by dispatching and allocating available emergency resources. Several studies have adopted distributed generators (DGs) [4]-[6], energy storage systems [7], [8], and renewable energy sources [6]-[9] for reconfiguration and restoration of distribution systems. For example, a limited number of reconfiguration steps based on the DG start-up requirements were imposed in [5]. Two-level simulation-assisted sequential DSR considering frequency constraints was proposed in [10]. Although the above-mentioned studies have contributed to temporary restoration, they have excluded the repair of damaged components, being unsuitable for permanent solutions. Other studies have incorporated the dispatch of maintenance crews into DSR to repair damaged components. A two-stage stochastic programming method using mobile resources and repair crews to facilitate DSR was proposed in [11]. Repair crews and multiple types of energy resources were coordinated in an integrated optimization model for unbalanced DSR in [12].

It can be found that the traditional DSR focused on the restoration of the electric side, but the influence of the cyber side on DSR was not considered. With the rapid growth of CNs, the cyber and electric lines in modern distribution systems have become inextricably linked and deeply coupled [13]. Normally, the cyber function of a distribution system remains intact, and the fast DSR can be performed through network topology reconfiguration by remotely monitoring and controlling the remote-controlled switches (RCSs). However, CNs and ENs in modern distribution systems may be simultaneously disrupted by extreme events [14]. The damage to CN may lead to a single failure or even cascading failures of electric components. Hence, the influence of CNs on ENs should be considered before developing DSR strategies. The impact of cyber-physical interactions on system resilience during extreme events was investigated in [15]. After the cyber function in the CN was interrupted, the command center was incapable of monitoring the condition and performing normal control of the electric components (e.g., RCSs), resulting in a considerable delay in load restoration. Overall, the coupling between ENs and CNs must be considered in the DSR.

Because of the coupling between ENs and CNs, the collaborative restoration of cyber-physical distribution system (CPDS) is being actively explored. In [16], a coordinated recovery strategy for CPDS was proposed integrating the gridding method. Regarding recovery resources, electric maintenance crews (EMCs) and cyber maintenance crews (CMCs) can be included during the DSR to jointly restore ENs and CNs [17], [18]. In addition, emergency communication vehicles (ECVs) can establish wireless communication networks after extreme events and are used for the cyber restoration in distribution systems. In [19], an emergency communication sector was established by optimally dispatching ECVs that can boost the DSR. ECVs have good application prospects in cyber restoration to reach the RCSs that need to be closed, temporarily restore the cyber function of RCSs, and ensure that they can be closed successfully. Similarly, small drone cells for wireless cyber restoration and DSR strategies were developed in [20]. However, the abovementioned studies considered only one type of dispatchable resources (CMCs, ECVs, or drones) for restoring CNs, being inefficient for complete DSR.

Diverse dispatchable resources participate in DSR, especially considering the coupling between ENs and CNs. The mobile resources must be dispatched to desired locations to complete their tasks through a traffic network (TN). The travel time of dispatchable resources is a critical factor of DSR. Based on the road parameters in the TN, it is realistic and reasonable to calculate the travel time of each dispatchable resource rather than determine it by predefined or random numbers [18], [21]. In [22], the multistage dynamic recovery strategies were devised considering an integrated energy system and TN. In [23] and [24], the optimization models for joint post-disaster DSR were developed considering co-dispatching with electric buses in the TN.

A DSR framework that considers the interdependence among ENs, CNs, and TNs can capture complex dynamics and interactions in modern distribution systems. Analyzing and solving DSR on this basis may provide system operators and planners with comprehensive and realistic strategies.

Overall, DSR after extreme events faces three main challenges.

1) Capturing information interactions among ENs, CNs, and TNs during DSR for establishing a sequential recovery framework based on the coupling of the three networks.

2) Quantifying and determining the scope of cyber failures in a CN and analyzing their impacts on load restoration for modern distribution systems.

3) Fully using diverse dispatchable resources and developing co-dispatching strategies for collaborative restoration of ENs and CNs to accelerate DSR.

Motivated by these challenges, we propose the DSR framework, as shown in Fig. 1, which provides three novel solutions. First, we introduce co-dispatching strategies for the three recovery resources. EMCs repair damaged electric lines, whereas CMCs and ECVs cooperate to restore the cyber function of RCSs by repairing damaged cyber lines or establishing wireless communications, which may support DSR. Second, a "cyber blind area" is defined as the cyber nodes that have lost the cyber function owing to the failure of cyber lines in the CN. As the information from cyber blind areas is intended to be transmitted to the ENs, the RCSs stop operating normally. Consequently, the cyber restora-

tion cannot directly lead to load restoration, and the dispatching of EMCs should be conducive to recovering the RCSs. Third, we model the TN in detail and combine the Floyd algorithm to calculate the travel time of each recovery resource during task execution in ENs and CNs.

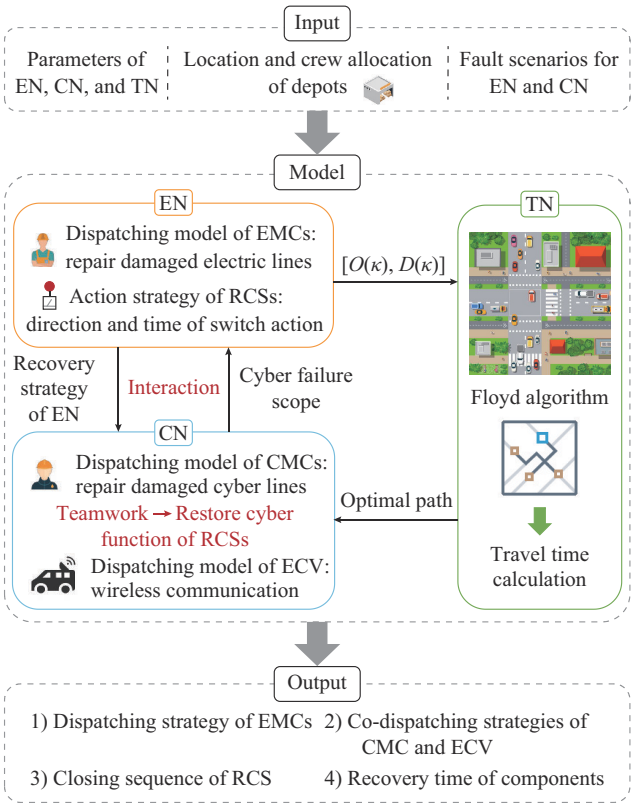

Fig. 1. Diagram of proposed DSR framework.

The main contributions of this study can be summarized as follows.

1) Considering the impact of CNs on post-disaster DSR, we propose a sequential recovery framework based on the coupling of ENs, CNs, and TNs incorporating the collaborative restoration of ENs and CNs with three dispatchable resources (EMCs, CMCs, and ECVs), and the travel time is calculated by the TN.

2) An intelligent algorithm is developed for searching cyber blind areas. The algorithm identifies cyber failures that have led to loss of the cyber function in the CN. In addition, it contributes to determining the cyber recovery time in DSR.

3) We propose a recovery mechanism to collaboratively dispatch multiple resources for restoring the same type of failure. As the CMCs and ECVs can collaborate to restore the cyber function of RCSs in different ways, the load restoration of distribution system can be accelerated.

The remainder of this paper is organized as follows. Section II describes the DSR framework considering ENs and CNs. In Section III, we present the corresponding solution methods. In Section IV, the proposed models in our DSR framework are tested, and the corresponding numerical results are discussed. Finally, conclusions are drawn in Section V.

II. DSR Framework Considering ENs and CNs

The dispatching models of EMCs, CMCs, and ECVs are first presented followed by the formation of the cyber blind area and recovery time model. Next, the DSR model with coupling of CN and EN and interdependence between the sub-models are detailed. Finally, the objective function and constraints of the co-optimization model are summarized.

A. Dispatching Models of EMCs, CMCs, and ECVs

EMCs and CMCs are the two main types of maintenance crews for repairing damaged electric and cyber lines, respectively. In addition, ECVs can restore the cyber function of RCSs by establishing wireless communication networks. Their dispatching models are aimed to determine the target paths and timetables for completing repair or recovery tasks. The dispatch models for the three dispatchable resources can be divided into target paths and timetables.

1) Target Path Problem

The target path problem is modeled to ensure that the travel of each dispatchable resource satisfies the following basic behavior logic rules.

$$\sum_{D(\kappa)} z_{d(\kappa),D(\kappa),\kappa} = \sum_{O(\kappa)} z_{O(\kappa),d(\kappa),\kappa} = 1 \quad \forall \kappa \tag{1}$$

$$\sum_{D(\kappa)} z_{D/d(\kappa),D(\kappa),\kappa} = \sum_{O(\kappa)} z_{O(\kappa),D/d(\kappa),\kappa} = 0 \quad \forall \kappa \tag{2}$$

$$\sum_{D(\kappa)} z_{O(\kappa),D(\kappa),\kappa} = \sum_{O(\kappa)} z_{O(\kappa),D(\kappa),\kappa} \le 1 \quad \forall \kappa \tag{3}$$

If $\kappa = emc$, $O(\kappa) \in V_{emc}^{\mathrm{DN}}$, $D(\kappa) \in V_{emc}^{\mathrm{DN}}$. The analogous relations apply to $\kappa = cmc$ and $\kappa = ecv$.

Constraints (1) and (2) indicate that dispatchable resource κ is required to leave and return to the depot ($d(\kappa)$) that it belongs to and cannot pass through other depots ($D/d(\kappa)$) at the beginning and end of the DSR tasks. In constraint (3), after a dispatchable resource reaches a non-depot vertex to complete the task, it leaves that vertex.

$$\sum_{emc}\sum_{m} z_{m,n,emc} = 1 \quad m \in V_{emc}^{\mathrm{EN}}, \forall n \in V_{emc}^{\mathrm{EN}}/D \tag{4}$$

$$\begin{cases} \sum_{ecv}\sum_{e} z_{e,f,ecv} \le 1 \quad e \in V_{ecv}^{\mathrm{EN}}, \forall f \in V_{ecv}^{\mathrm{EN}}/D \\ \sum_{cmc}\sum_{p} z_{p,q,cmc} \le 1 \quad p \in V_{cmc}^{\mathrm{CN}}, \forall q \in V_{cmc}^{\mathrm{CN}}/D \end{cases} \tag{5}$$

Constraints (4) and (5) limit the number of recovery resources required to perform tasks at a specific vertex. For EMCs, all damaged electric lines must be repaired, and the damaged electric line in one vertex can only be repaired by one EMC. These two aspects are considered in constraint (4).

Constraint (5) differs from (4) in two aspects. First, not all the damaged cyber lines or RCSs must be repaired or closed. Second, the main task of the CMCs and ECVs is restoring the cyber function of the RCSs to ensure that they can be timely closed when needed. Specifically, an RCS cannot operate properly because the cyber function is lost owing to the damage to cyber lines. There are two ways to restore the cyber function: ① CMCs repair the relevant damaged cyber lines; and ② an ECV travels to the RCS for temporarily restoring the cyber function. Thus, the dispatching

strategies of the CMCs and ECVs should be properly selected.

2) Timetable Problem

The timetable problem is modeled to represent the time relations of the three dispatchable resources during the DSR progress.

First, the timetable problem of EMCs and CMCs is modeled as:

$$\begin{cases} t^{\text{reach}}_{D(\kappa),\kappa} \le t^{\text{reach}}_{O(\kappa),\kappa} + T^{\text{rep}}_{O(\kappa),\kappa} + T^{\text{tr}}_{O(\kappa),D(\kappa),\kappa} + M(1 - z_{O(\kappa),D(\kappa),\kappa}) \\ t^{\text{reach}}_{D(\kappa),\kappa} \ge t^{\text{reach}}_{O(\kappa),\kappa} + T^{\text{rep}}_{O(\kappa),\kappa} + T^{\text{tr}}_{O(\kappa),D(\kappa),\kappa} - M(1 - z_{O(\kappa),D(\kappa),\kappa}) \end{cases} \quad \forall \kappa \in \{emc, cmc\} \tag{6}$$

$$0 \le t^{\text{reach}}_{D(\kappa),\kappa} \le M \sum_{O(\kappa)} z_{O(\kappa),D(\kappa),\kappa} \quad \forall \kappa \in \{emc, cmc\} \tag{7}$$

$$t^{\text{comp}}_{D(\kappa)} = \sum_{\kappa} \left(t^{\text{reach}}_{D(\kappa),\kappa} + T^{\text{rep}}_{D(\kappa),\kappa} \sum_{O(\kappa)} z_{O(\kappa),D(\kappa),\kappa} \right) \quad \forall \kappa \in \{emc, cmc\} \tag{8}$$

Constraint (6) depicts the time relation of dispatchable resource κ traveling between two vertices to perform the repair tasks. Specifically, if κ travels from $O(\kappa)$ to $D(\kappa)$, i.e., $z_{O(\kappa),D(\kappa),\kappa}=1$, κ will arrive at $D(\kappa)$ at time $t^{\text{reach}}_{D(\kappa),\kappa} = t^{\text{reach}}_{O(\kappa),\kappa} + T^{\text{rep}}_{O(\kappa),\kappa} + T^{\text{tr}}_{O(\kappa),D(\kappa),\kappa}$. For example, if $\kappa = emc$ and $z_{m,n,emc}=1$, the time relation is $t^{\text{reach}}_{n,emc} = t^{\text{reach}}_{m,emc} + T^{\text{rep}}_{m,emc} + T^{\text{tr}}_{m,n,emc}$. We set $t^{\text{reach}}_{O(\kappa),\kappa}$ to be 0 in (6) if $O(\kappa) \in D$. However, $t^{\text{reach}}_{D(\kappa),\kappa}$ equals 0 if κ is not dispatched to $D(\kappa)$ for repair work, i.e., $\sum_{O(\kappa)} z_{O(\kappa),D(\kappa),\kappa} = 0$, which is limited by (7). Constraint (8) indicates that if κ travels to $D(\kappa)$ and repairs the corresponding damaged lines, i.e., $\sum_{O(\kappa)} z_{O(\kappa),D(\kappa),\kappa} = 1$, the relation between the arrival time $t^{\text{reach}}_{D(\kappa),\kappa}$ and the repair completion time $t^{\text{comp}}_{D(\kappa)}$ of $D(\kappa)$ satisfies $t^{\text{comp}}_{D(\kappa)} = t^{\text{reach}}_{D(\kappa),\kappa} + T^{\text{rep}}_{D(\kappa),\kappa}$. For example, for $\kappa = emc$ and $\sum_{m} z_{m,n,emc} = 1$, the relation is given by $t^{\text{comp}}_{n} = t^{\text{reach}}_{n,emc} + T^{\text{rep}}_{n,emc}$. It should be noted that the value of $t^{\text{comp}}_{D(\kappa)}$ equals 0 if $D(\kappa) \in D$.

Second, the timetable problem of ECVs is described as:

$$\begin{cases} t^{\text{reach}}_{f,ecv} \le t^{\text{leave}}_{e,ecv} + T^{\text{tr}}_{e,f,ecv} + M(1 - z_{e,f,ecv}) \\ t^{\text{reach}}_{f,ecv} \ge t^{\text{leave}}_{e,ecv} + T^{\text{tr}}_{e,f,ecv} - M(1 - z_{e,f,ecv}) \end{cases} \quad \forall e,f \in V^{\text{EN}}_{ecv} \tag{9}$$

$$\begin{cases} 0 \le t^{\text{reach}}_{e,ecv} \le M \sum_{f} z_{f,e,ecv} \\ 0 \le t^{\text{leave}}_{e,ecv} \le M \sum_{f} z_{f,e,ecv} \end{cases} \quad f \in V^{\text{EN}}_{ecv}, \forall e \in V^{\text{EN}}_{ecv} \tag{10}$$

Constraint (9) indicates that if *ecv* travels from vertices e to f, i.e., $z_{e,f,ecv}=1$, for recovering an RCS, *ecv* arrives at vertex f at time $t^{\text{reach}}_{f,ecv} = t^{\text{leave}}_{e,ecv} + T^{\text{tr}}_{e,f,ecv}$. However, the arrival time $t^{\text{reach}}_{e,ecv}$ and departure time $t^{\text{leave}}_{e,ecv}$ of vertex e are both 0 if *ecv* is not dispatched to vertex e for recovery, i.e., $\sum_{f} z_{f,e,ecv} = 0$, as set by constraint (10). Moreover, $t^{\text{leave}}_{e,ecv}$ equals 0 if vertex e is a depot.

$$\begin{cases} t^{\text{leave}}_{e,ecv} \le t^{\text{reach}}_{e,ecv} + T^{\text{stay}}_{e,ecv} + M\left(1 - \sum_{f} z_{f,e,ecv}\right) \\ t^{\text{leave}}_{e,ecv} \ge t^{\text{reach}}_{e,ecv} + T^{\text{stay}}_{e,ecv} - M\left(1 - \sum_{f} z_{f,e,ecv}\right) \end{cases} \quad f \in V^{\text{EN}}_{ecv}, \forall e \in V^{\text{EN}}_{ecv}/D, \forall ecv \tag{11}$$

This is different from EMCs that leave the vertex immediately after repairing the damaged lines. During the deployment of the ECV to a vertex, the cyber function of the RCS is temporarily restored, and the switch can operate normally because wireless communications are available during that period. Constraint (11) ensures that if *ecv* travels to vertex e and temporarily restores the cyber function of an RCS, i.e., $\sum_{f} z_{f,e,ecv} = 1$, the relation between arrival time $t^{\text{reach}}_{e,ecv}$ and departure time $t^{\text{leave}}_{e,ecv}$ of vertex e satisfies $t^{\text{leave}}_{e,ecv} = t^{\text{reach}}_{e,ecv} + T^{\text{stay}}_{e,ecv}$.

$$T^{\text{stay}}_{e,ecv} \ge T^{\text{RS}}_{a,b} + T^{\text{op}}_{ecv} - M\left(1 - \sum_{f} z_{f,e,ecv}\right) \tag{12}$$

$$0 \le T^{\text{stay}}_{e,ecv} \le M \sum_{f} z_{f,e,ecv} \quad f \in V^{\text{EN}}_{ecv}, (a,b) \in V^{\text{RS}}, \forall e \in V^{\text{EN}}_{ecv}/D, \forall ecv \tag{13}$$

During the deployment of *ecv* at vertex e ($T^{\text{stay}}_{e,ecv}$), the operation time of *ecv* (T^{op}_{ecv}) and closing time of RCS ($T^{\text{RS}}_{a,b}$) should be considered. Thus, $T^{\text{stay}}_{e,ecv}$ is at least $T^{\text{op}}_{ecv} + T^{\text{RS}}_{a,b}$, as indicated by constraint (12). In addition, constraint (13) indicates that $T^{\text{stay}}_{e,ecv}$ should be zero if no *ecv* is dispatched to vertex e, i.e., $\sum_{f} z_{f,e,ecv} = 0$.

B. Models for Cyber Blind Area and Cyber Recovery Time

We use the topology-consistent CN in the CPDS introduced in [25]. Thus, the ENs and CNs have the same topology (i.e., each electric node is equipped with a cyber node), and the CN has a radial topology. Then, we define the concept of a cyber blind area to indicate the cyber nodes that have lost the cyber function owing to the failure of cyber lines in the CN, as shown in Fig. 2.

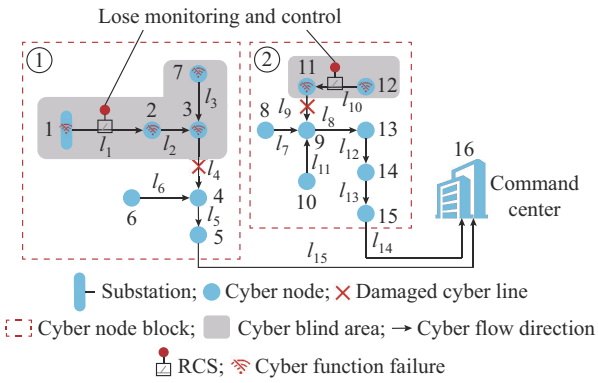

Fig. 2. Diagram of cyber blind area.

Specifically, when a cyber line is damaged due to an extreme event in a CN, the downstream cyber nodes connected to the line lose contact with the command center, causing some electric nodes within the range of the EN to lose monitoring and control capabilities. The cyber blind area causes the RCSs to lose control and fail to operate normally. We consider that the cyber nodes controlled by a command center constitute a cyber node block.

We propose an intelligent algorithm to search all cyber blind areas and their cyber nodes, as described in Algorithm 1.

Algorithm 1: search of cyber blind areas and their cyber nodes

Input: CN topology, V^{DCL}, and N_a
Output: C and N_c
1: Establish adjacency matrix based on CN topology (represent a directed graph with edges pointing from a cyber node to its command center)
2: Set $c=1$
3: **for** all $l \in V^{\mathrm{DCL}}$ **do**
4: Obtain downstream node i of damaged cyber line l, and include it into cyber blind area c
5: Determine cyber node block a to which damaged cyber line l belongs, and find all cyber nodes in cyber node block a
6: **for** all $j \in N_a$ **do**
7: Apply Floyd algorithm to obtain the shortest path scheme P and its path length s from cyber nodes j to i in cyber node block a
8: **if** $P \neq \varnothing$ and $d \neq 0$ **then**
9: Bring the cyber node j in cyber node block a into cyber blind area c
10: **end if**
11: **end for**
12: $c=c+1$
13: **end for**

The set of cyber blind areas C and the cyber nodes contained in each area can be obtained using Algorithm 1. We apply the Floyd algorithm to generate the shortest path scheme and length between two nodes. The Floyd algorithm is detailed in [17].

When CMCs repair the damaged cyber lines, the cyber function of the cyber nodes and the observability and controllability of the corresponding electric nodes are restored. The cyber recovery time model is formulated as:

$$t_i^{\mathrm{CR}} = \max(t_{p(c)}^{\mathrm{comp}}) + M\left(numel(c) - \sum_{q}\sum_{p(c)}\sum_{cmc} z_{q,p(c),cmc}\right) \quad \forall i \in N_c, c \in C, p(c) \in V_{cmc}^{\mathrm{CN}}/D, q \in V_{cmc}^{\mathrm{CN}} \tag{14}$$

Equation (14) determines the cyber recovery time of cyber node i in cyber blind area c. In (14), we consider that multiple cyber lines may be damaged on the same feeder (cyber node i is included in multiple cyber blind areas), where $numel(c)$ indicates the number of cyber blind areas. The cyber function of cyber node i is restored if and only if all the upstream damaged cyber lines of the node on the same feeder are repaired, and t_i^{CR} equals $\max(t_{p(c)}^{\mathrm{comp}})$, which represents the maximum repair completion time for upstream damaged cyber lines on a feeder. Note that $p(c)$ denotes the damaged cyber lines causing cyber blind area c in vertex p. Otherwise, t_i^{CR} is set to be a large value. Additionally, t_i^{CR} is set to be 0 if cyber node i does not belong to a cyber blind area.

C. DSR Model

Considering the coupling of ENs and CNs, we solve the DSR problem by selecting and dispatching EMCs, CMCs, ECVs, and DGs, generating a sequential closing strategy for RCSs and gradually restoring the power supply. DSR can be divided into two parts: the energization strategy and operation constraints of the distribution system.

1) Energization Strategy

We model an energization strategy of the electric node blocks to obtain their energization path and timetable for DSR.

The energization path problem $z_{a,b}^{\mathrm{DSRM}}$ is defined to express whether the RCS between electric node blocks a and b is closed and the energization direction goes from a to b. The energization path of the electric node blocks is modeled as:

$$0 \le \sum_a \sum_b z_{a,b}^{\mathrm{DSRM}} \le numel(a) \quad a \in B^{\mathrm{sub}}, b \in B/B^{\mathrm{sub}} \tag{15}$$

$$\sum_a z_{a,b}^{\mathrm{DSRM}} = 0 \quad \forall b \in B^{\mathrm{sub}} \tag{16}$$

$$\sum_a z_{a,b}^{\mathrm{DSRM}} = 1 \quad \forall b \in B/B^{\mathrm{sub}} \tag{17}$$

$$\begin{cases} z_{a,b}^{\mathrm{DSRM}} \le 1 & a \text{ and } b \text{ are directly connected} \\ z_{a,b}^{\mathrm{DSRM}} = 0 & \text{otherwise} \end{cases} \tag{18}$$

Constraint (15) indicates that an energization path should start from the substation node block, and the maximum value cannot exceed the number of substation node blocks. Constraint (16) ensures that the energization path cannot pass through a substation node block. Constraint (17) limits the electric node block (excluding substation node block) that must be accessed by an energization path to ensure restoration of the power supply and radial operation. In addition, the value of $z_{a,b}^{\mathrm{DSRM}}$ is set by (18).

We determine the timetable of each DSR component, including the electric node blocks, loads, DGs, and RCSs. First, the energization time of the electric node blocks must satisfy the following constraints. In (19), the substation node block is energized at $t=0$, and (20) indicates that $t_b^{\mathrm{DSRM}} = t_{a,b}^{\mathrm{RS}}$ if $z_{a,b}^{\mathrm{DSRM}} = 1$.

$$t_a^{\mathrm{DSRM}} = 0 \quad a \in B^{\mathrm{sub}} \tag{19}$$

$$t_{a,b}^{\mathrm{RS}} - M(1 - z_{a,b}^{\mathrm{DSRM}}) \le t_b^{\mathrm{DSRM}} \le t_{a,b}^{\mathrm{RS}} + M(1 - z_{a,b}^{\mathrm{DSRM}}) \quad \forall b \in B/B^{\mathrm{sub}}, (a,b) \in V^{\mathrm{RS}} \tag{20}$$

Second, we limit the closing completion time of the RCSs. Because an RCS can only be closed when the cyber function on both sides is intact, as described in Section II-A, its closing completion time is related to ECVs and CMCs. Binary variables u_{rs}^{ECV} and u_{rs}^{CMC} indicate whether the cyber function of RCS rs is restored by ECVs or CMCs. If the RCS connects electric node blocks a and b and the energization direction goes from a to b, its closing completion time is determined by constraints (21)-(26).

$$\begin{cases} t_{a,b}^{\mathrm{RS}} \ge -M(z_{a,b}^{\mathrm{DSRM}} + z_{b,a}^{\mathrm{DSRM}}) \\ t_{a,b}^{\mathrm{RS}} \le M(z_{a,b}^{\mathrm{DSRM}} + z_{b,a}^{\mathrm{DSRM}}) \end{cases} \quad \forall (a,b) \in V^{\mathrm{RS}} \tag{21}$$

$$0 \le t_{a,b}^{\mathrm{RS}} \le M(1 - z_{b,a}^{\mathrm{DSRM}}) \quad \forall (a,b) \in V^{\mathrm{RS}} \tag{22}$$

$$u_{rs}^{\mathrm{ECV}} + u_{rs}^{\mathrm{CMC}} = z_{a,b}^{\mathrm{DSRM}} + z_{b,a}^{\mathrm{DSRM}} \le 1 \quad \forall rs \in V^{\mathrm{RS}}, (a,b) \in V^{\mathrm{RS}} \tag{23}$$

$$t_{a,b}^{\mathrm{RS}} \ge t_a^{\mathrm{DSRM}} + T_{a,b}^{\mathrm{RS}} - M(1 - z_{a,b}^{\mathrm{DSRM}}) \tag{24}$$

$$\begin{cases} t_{a,b}^{\mathrm{RS}} \ge \left[\sum_{ecv} t_{e,ecv}^{\mathrm{reach}} + T_{ecv}^{\mathrm{op}} + T_{a,b}^{\mathrm{RS}} - M(1 - z_{a,b}^{\mathrm{DSRM}})\right] u_{rs}^{\mathrm{ECV}} \\ t_{a,b}^{\mathrm{RS}} \le \sum_{ecv} t_{e,ecv}^{\mathrm{reach}} + M(2 - z_{a,b}^{\mathrm{DSRM}} - u_{rs}^{\mathrm{ECV}}) \end{cases} \quad \forall rs \in V^{\mathrm{RS}}, (a,b) \in V^{\mathrm{RS}}, e \in V^{\mathrm{RS}} \tag{25}$$

$$t_{a,b}^{\mathrm{RS}} \ge [\max(t_i^{\mathrm{CR}}, t_j^{\mathrm{CR}}) + T_{a,b}^{\mathrm{RS}} - M(1 - z_{a,b}^{\mathrm{DRSM}})] u_{rs}^{\mathrm{CMC}} \quad \forall rs \in V^{\mathrm{RS}}, (a,b) \in V^{\mathrm{RS}}, (i,j) \in V^{\mathrm{RS}} \tag{26}$$

Specifically, $t_{a,b}^{\mathrm{RS}}$ equals 0 if the energization direction goes from b to a or if the RCS is not required to be closed, as described in (21) and (22). The cyber function of an RCS can only be restored by an ECV or CMC, and there can only be one energization direction between a and b. Formula (24) indicates the relation between $t_{a,b}^{\mathrm{RS}}$ and t_a^{DSRM}, and $t_{a,b}^{\mathrm{RS}}$ is determined by (25) if the cyber function of RCS rs is temporarily restored by an ECV. Otherwise, it is determined by (26), which is restored by the CMCs. In (26), (i, j) are electric nodes on both sides of the RCS.

Let us analyze the case where the energization direction goes from a to b in (21), (22), and (24)-(26). Before the result is obtained, the energization direction between the electric node blocks cannot be determined. Therefore, the constraints should be added such that the energization direction goes from b to a, whose analysis is the same as that from a to b.

Third, the loads of all electric nodes contained in the electric node block are restored when the electric node block is energized. Consequently, t_i^{R} can be determined as:

$$t_i^{\mathrm{R}} = t_a^{\mathrm{DSRM}} \quad \forall i \in N_a, a \in B \tag{27}$$

2) Operation Constraints

The operation conditions of EN change only when the loads or DGs are energized. Therefore, it is not essential to check the operation constraints at every time point. Variables $z_{i,t}^{\mathrm{ES}}$, $z_{a,b,t}^{\mathrm{ES}}$, and $z_{i,j,t}^{\mathrm{ES}}$ are defined to represent the energization statuses of the electric nodes, RCSs, and electric lines, respectively, as:

$$z_{i,t}^{\mathrm{ES}} = \begin{cases} 0 & t < t_i^{\mathrm{R}} \\ 1 & \text{else} \end{cases} \quad \forall i \in N, \forall t \in T^{\mathrm{R}} \tag{28}$$

$$z_{a,b,t}^{\mathrm{ES}} = \begin{cases} 0 & z_{a,b}^{\mathrm{DSRM}} = z_{b,a}^{\mathrm{DSRM}} = 0 \\ 0 & z_{a,b}^{\mathrm{DSRM}} + z_{b,a}^{\mathrm{DSRM}} = 1 \text{ and } t < t_{a,b}^{\mathrm{RS}} \\ 1 & z_{a,b}^{\mathrm{DSRM}} + z_{b,a}^{\mathrm{DSRM}} = 1 \text{ and } t \geq t_{a,b}^{\mathrm{RS}} \end{cases} \quad \forall (a,b) \in V^{\mathrm{RS}} \tag{29}$$

$$z_{i,j,t}^{\mathrm{ES}} = \begin{cases} 0 & t < t_a^{\mathrm{DRSM}} \\ 1 & \text{else} \end{cases} \quad \forall a \in B, \forall (i,j) \in L_a, \forall t \in T^{\mathrm{R}} \tag{30}$$

We adopt a linearized DistFlow model with the following constraints as:

$$\begin{cases} \sum_{j \in ds(i)} P_{i,j,t} - \sum_{j \in us(i)} P_{j,i,t} = P_{i,t}^{\mathrm{G}} - P_i^{\mathrm{load}} z_{i,t}^{\mathrm{ES}} \\ \sum_{j \in ds(i)} Q_{i,j,t} - \sum_{j \in us(i)} Q_{j,i,t} = Q_{i,t}^{\mathrm{G}} - Q_i^{\mathrm{load}} z_{i,t}^{\mathrm{ES}} \end{cases} \quad \forall i \in N, \forall t \in T^{\mathrm{R}} \tag{31}$$

$$\begin{cases} U_{i,t} - U_{j,t} \leq (R_{i,j} P_{i,j,t} + X_{i,j} Q_{i,j,t})/U_0 + M(1 - z_{i,j,t}^{\mathrm{ES}}) \\ U_{i,t} - U_{j,t} \geq (R_{i,j} P_{i,j,t} + X_{i,j} Q_{i,j,t})/U_0 - M(1 - z_{i,j,t}^{\mathrm{ES}}) \end{cases} \quad \forall (i,j) \in L \tag{32}$$

$$\begin{cases} -P_{i,j}^{\max} z_{i,j,t}^{\mathrm{ES}} \leq P_{i,j,t} \leq P_{i,j}^{\max} z_{i,j,t}^{\mathrm{ES}} \\ -Q_{i,j}^{\max} z_{i,j,t}^{\mathrm{ES}} \leq Q_{i,j,t} \leq Q_{i,j}^{\max} z_{i,j,t}^{\mathrm{ES}} \end{cases} \quad \forall (i,j) \in L, \forall t \in T^{\mathrm{R}} \tag{33}$$

$$\begin{cases} 0 \leq P_{i,t}^{\mathrm{G}} \leq P_i^{\max} z_{i,t}^{\mathrm{ES}} \\ 0 \leq Q_{i,t}^{\mathrm{G}} \leq Q_i^{\max} z_{i,t}^{\mathrm{ES}} \end{cases} \quad \forall i \in N, \forall t \in T^{\mathrm{R}} \tag{34}$$

$$U_i^{\min} z_{i,t}^{\mathrm{ES}} \leq U_{i,t} \leq U_i^{\max} z_{i,t}^{\mathrm{ES}} \quad \forall i \in N, \forall t \in T^{\mathrm{R}} \tag{35}$$

$$\sum_{t \in T^{\mathrm{R}}} z_{i,t}^{\mathrm{ES}} \geq 1 \quad \forall i \in N \tag{36}$$

Constraint (31) represents the power balance of the electric node. Constraint (32) limits the voltage drop of line ij. Constraints (33)-(35) define the maximum and minimum limits of the line power flow, node generation capacity, and node voltage, respectively. Constraint (36) ensures that all the loads are restored.

D. Constraints of Coupling Relations

First, we consider the relation between the dispatching of ECVs and RCSs. The ECVs skip RCSs that do not need to be closed or RCSs with an intact cyber function on both sides, as shown in constraints (37) and (38).

$$\sum_e \sum_{ecv} z_{e,f,ecv} \leq z_{m,n}^{\mathrm{DSRM}} + z_{n,m}^{\mathrm{DSRM}} \quad \forall f \in V^{\mathrm{RS}}, (m,n) \in V^{\mathrm{RS}} \tag{37}$$

$$\sum_e \sum_{ecv} z_{e,f,ecv} = 0 \quad \forall f \in V_{\mathrm{int}}^{\mathrm{RS}} \tag{38}$$

Second, we fully consider the relation between the repair completion time of damaged lines and energization time of the electric node block to ensure the safety of EMCs in repairing damaged electric lines. The electric node block can be energized only after all the damaged lines are repaired, as formulated in constraint (39).

$$t_a^{\mathrm{DSRM}} \geq t_m^{\mathrm{comp}} + \sum_b T_{b,a}^{\mathrm{RS}} z_{b,a}^{\mathrm{DSRM}} \quad \forall m \in L_a^{\mathrm{EMC}} \tag{39}$$

E. Co-optimization Recovery Model

A co-optimization recovery model restores the power supply of all loads and minimizes the load curtailment during the recovery process. The objective function is designed to minimize the load curtailment as:

$$\min \sum_{i \in N} \omega_i t_i^{\mathrm{R}} P_i^{\mathrm{load}} \tag{40}$$

The objective function is subject to the following constraints: ① dispatch constraints for EMCs, CMCs, and ECVs (1) - (13); ② cyber recovery time of nodes in cyber blind area (14); ③ energization path and timetable in the DSR model (15) - (27); ④ operation constraints (28) - (36); and ⑤ constraints of coupling relations (37)-(39).

III. Solution Methods

To solve the proposed model efficiently, we adopt three methods: ① fault allocation reducing the computational burden; ② TN topology to calculate the traffic time of the three dispatchable resources; and ③ nonlinear constraints for solving after linearization.

A. Fault Allocation

In the proposed model, the EMCs and CMCs are dispatched to perform repair tasks at each destination. The numerous resulting binary variables increase the computational burden. Hence, based on proximity, we adopt fault allocation to assign the repair tasks of the damaged electric and cyber lines to each depot.

The fault allocation for damaged electric lines can be described by (41)-(43).

$$\min \sum_d \sum_m l_{d,m} z_{d,m}^{\mathrm{FAM}} \tag{41}$$

s.t.

$$\sum_{d} z_{d,m}^{\mathrm{FAM}} = 1 \quad \forall m \in V_{emc}^{\mathrm{EN}}/D \tag{42}$$

$$\sum_{n} \sum_{emc \in d(m)} z_{n,m,emc} = 1 \quad \forall m \in V_{emc}^{\mathrm{EN}}/D \tag{43}$$

Objective function (41) indicates that the repair tasks of damaged electric lines are allocated to each station according to proximity. Constraint (42) ensures that each damaged electric line is assigned to a depot. Constraint (43) indicates that, for a repair task at vertex m, the EMC in assigned depot $d(m)$ must complete the task.

Similarly, the fault allocation for damaged cyber lines can be described by (44)-(46). Constraint (46) is different from constraint (43) because not all damaged cyber lines must be repaired.

$$\min \sum_{d} \sum_{p} l_{d,p} z_{d,p}^{\mathrm{FAM}} \tag{44}$$

s.t.

$$\sum_{d} z_{d,p}^{\mathrm{FAM}} = 1 \quad \forall p \in V_{cmc}^{\mathrm{CN}}/D \tag{45}$$

$$\begin{cases} \sum_{q} \sum_{cmc \in d(p)} z_{q,p,cmc} \le 1 \\ \sum_{q} \sum_{cmc \notin d(p)} z_{q,p,cmc} = 0 \end{cases} \quad \forall p \in V_{cmc}^{\mathrm{CN}}/D \tag{46}$$

B. Traffic Time Calculation

We model the TN by simulating the actual road conditions to determine the travel time and ensure the feasibility of the optimization strategy.

The TN topology can be modeled by an undirected graph, $G=(N_{\mathrm{T}}, L_{\mathrm{T}})$. The adjacency matrix $\boldsymbol{A}_{\mathrm{road}}$ is established to reflect the connections in the TN and determined by (47). This matrix is primarily used in the Floyd algorithm.

$$\boldsymbol{A}_{\mathrm{road}} = \begin{bmatrix} a_{11} & a_{12} & \cdots & a_{1j} \\ a_{21} & a_{22} & \cdots & a_{2j} \\ \vdots & \vdots & & \vdots \\ a_{i1} & a_{i2} & \cdots & a_{ij} \end{bmatrix} \tag{47}$$

where $a_{ij} = a_{ji} = \begin{cases} l_{ij} & (i,j) \in L_{\mathrm{T}} \\ 0 & i=j \text{ and } i,j \in N_{\mathrm{T}}. \\ \inf & (i,j) \notin L_{\mathrm{T}} \end{cases}$

The traffic roads in L_{T} are divided into three types: trunk roads, secondary trunk roads, and expressways. The relation between travel speed and road capacity of different road types is determined by the road impedance function given by:

$$\begin{cases} v_{ij}(t) = v_{ij,0}/[1 + (h_{ij}(t)/h_{ij}^{\max})^{\sigma}] \\ \sigma = r + s(h_{ij}(t)/h_{ij}^{\max})^{\delta} \end{cases} \tag{48}$$

The shortest path and distance l_{ij} between any two nodes i and j can be obtained using the Floyd algorithm. Finally, according to the relation between road distance l_{ij} and travel speed $v_{ij}(t)$, the traffic route time $T_{m,n,emc}^{\mathrm{tr}}$, $T_{e,f,ecv}^{\mathrm{tr}}$, and $T_{p,q,cmc}^{\mathrm{tr}}$ can be calculated.

C. Linearization

In constraint (25), $\sum_{ecv} t_{e,ecv}^{\mathrm{reach}}$ is a continuous variable, and $M(1-z_{a,b}^{\mathrm{DSRM}})$ and u_{rs}^{ECV} are binary variables. Hence, the first formula of constraint (25) is nonlinear and can be linearized into (49)-(51) by introducing auxiliary variables $t_{rs}^{\mathrm{reach,ECV}}$ and z_{rs}^{ECV}. A similar formulation can be derived for constraint (26).

$$t_{a,b}^{\mathrm{RS}} \ge t_{rs}^{\mathrm{reach,ECV}} + u_{rs}^{\mathrm{ECV}}(T_{ecv}^{\mathrm{op}} + T_{a,b}^{\mathrm{RS}}) - M z_{rs}^{\mathrm{ECV}} \tag{49}$$

$$\begin{cases} t_{rs}^{\mathrm{reach,ECV}} \le M u_{rs}^{\mathrm{ECV}} \\ t_{rs}^{\mathrm{reach,ECV}} \le \sum_{ecv} t_{e,ecv}^{\mathrm{reach}} \\ t_{rs}^{\mathrm{reach,ECV}} \ge \sum_{ecv} t_{e,ecv}^{\mathrm{reach}} - M(1-u_{rs}^{\mathrm{ECV}}) \end{cases} \quad 0 \le t_{rs}^{\mathrm{reach,ECV}} \le M \tag{50}$$

$$\begin{cases} z_{rs}^{\mathrm{ECV}} \le 1 - z_{a,b}^{\mathrm{DSRM}} & z_{rs}^{\mathrm{ECV}} \le u_{rs}^{\mathrm{ECV}} \\ z_{rs}^{\mathrm{ECV}} \ge u_{rs}^{\mathrm{ECV}} - z_{a,b}^{\mathrm{DSRM}} & 0 \le z_{rs}^{\mathrm{ECV}} \le 1 \end{cases} \tag{51}$$

To determine the binary variables in constraints (28)-(30), we obtain the corresponding linearization formulas (52)-(54).

$$(t - t_i^{\mathrm{R}} + \zeta)/M \le z_{i,t}^{\mathrm{ES}} \le (t - t_i^{\mathrm{R}} + \zeta)/M + 1 \tag{52}$$

$$\begin{cases} z_{a,b,t}^{\mathrm{ES}} \ge (z_{a,b}^{\mathrm{DSRM}} + z_{b,a}^{\mathrm{DSRM}})(t - t_{a,b}^{\mathrm{RS}} + \zeta)/M \\ z_{a,b,t}^{\mathrm{ES}} \le (z_{a,b}^{\mathrm{DSRM}} + z_{b,a}^{\mathrm{DSRM}})(t - t_{a,b}^{\mathrm{RS}} + \zeta)/M + (z_{a,b}^{\mathrm{DSRM}} + z_{b,a}^{\mathrm{DSRM}}) \end{cases} \tag{53}$$

$$(t - t_a^{\mathrm{DSRM}} + \zeta)/M \le z_{i,j,t}^{\mathrm{ES}} \le (t - t_a^{\mathrm{DSRM}} + \zeta)/M + 1 \tag{54}$$

Formula (53) can be linearized using (55) and (56) by introducing auxiliary variable $\alpha_{a,b}$.

$$\alpha_{a,b}/M \le z_{a,b,t}^{\mathrm{ES}} \le \alpha_{a,b}/M + z_{a,b}^{\mathrm{DSRM}} + z_{b,a}^{\mathrm{DSRM}} \tag{55}$$

$$\begin{cases} -M(z_{a,b}^{\mathrm{DSRM}} + z_{b,a}^{\mathrm{DSRM}}) \le \alpha_{a,b} \le M(z_{a,b}^{\mathrm{DSRM}} + z_{b,a}^{\mathrm{DSRM}}) \\ \alpha_{a,b} \le t - t_{a,b}^{\mathrm{RS}} + \zeta + M(1 - z_{a,b}^{\mathrm{DSRM}} - z_{b,a}^{\mathrm{DSRM}}) \\ \alpha_{a,b} \ge t - t_{a,b}^{\mathrm{RS}} + \zeta - M(1 - z_{a,b}^{\mathrm{DSRM}} - z_{b,a}^{\mathrm{DSRM}}) \end{cases} \tag{56}$$

IV. Case Studies

In this section, we verify the effectiveness and superiority of the proposed DSR framework on the modified IEEE 33-node and 123-node test systems. The operation time of the ECV T_{ecv}^{op} is set to be 10 min. For the traffic parameters, we assume that the road capacity of all types of roads is consistent at all time. The zero flow speed of roads ($v_{ij,0}$) is set to be 60 km/h. The road coefficients r, s, and δ of the trunk road are set to be 1.726, 3.15, and 3, whereas those of the secondary trunk road and expressway are set to be 2.076, 2.870, and 3, respectively. In addition, the road saturation coefficients of the trunk road, secondary trunk road, and expressway are taken as random numbers in 0.6-0.8, 0.5-0.7, and 0.4-0.6, respectively. The simulations are implemented using Gurobi 9.5.2 on MATLAB R2018 running on a desktop computer equipped with an Intel Core i5-10500H processor, 16 GB RAM, and 64-bit operating system.

A. IEEE 33-node Test System

The system voltage for the IEEE 33-node test system is 12.66 kV, with a total load demand of (3.715 + j2.30)MVA [26]. The EN and CN adopt the same topology, as shown in Fig. 3. Relevant TN topology are shown in Fig. 4. Virtual nodes are used only to represent the geographic location of the RCSs.

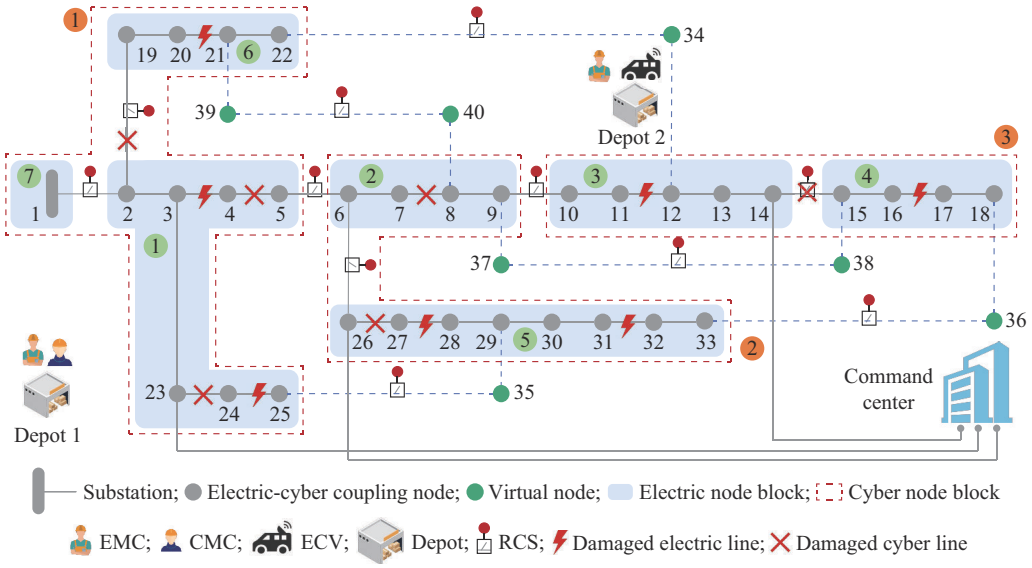

Fig. 3. Modified IEEE 33-node test system.

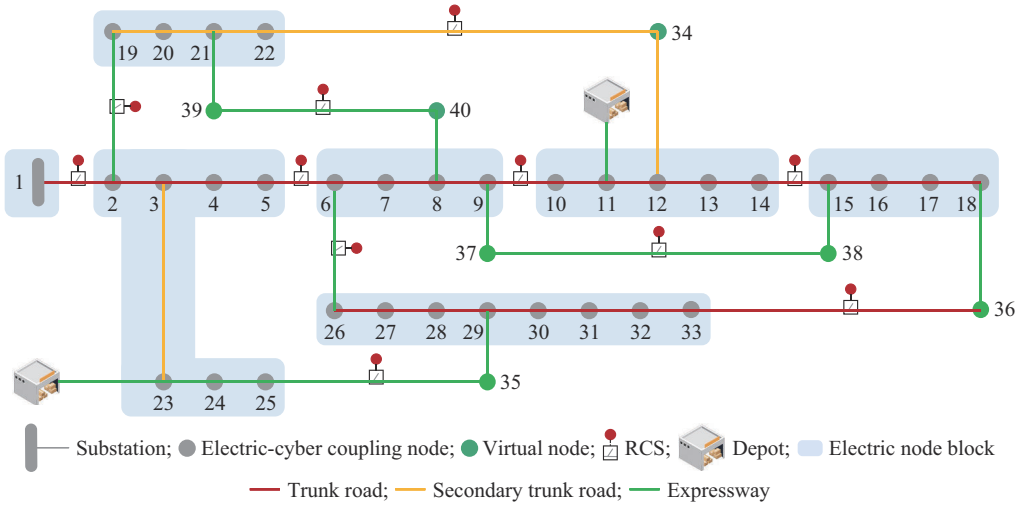

Fig. 4. TN topology for IEEE 33-node test system.

The IEEE 33-node test system is equipped with two depots, 11 RCSs, and one substation. To simulate a failure scenario and post-disaster recovery resources after extreme events, we consider seven damaged electric lines and six damaged cyber lines as a benchmark failure scenario. Depot 1 comprises one EMC and one CMC, whereas Depot 2 comprises one EMC and one ECV. For the EN and CN, the repair time of damaged electric and cyber lines is set to be 1.2 hours [17], and the closing time of an RCS is 5 min.

According to fault allocation (Section III-C), the damaged electric and cyber lines are assigned to the nearest depot, obtaining the results listed in Table I.

For the benchmark failure scenario, the proposed co-optimization model is solved in 15.43 s. The proposed strategies restore all the loads in 360 min, and the total restored energy reaches 9615.50 kWh. The travel paths and timetables for the three dispatchable resources are listed in Table II. The co-dispatching of three recovery resources and energized areas are shown in Fig. 5.

TABLE I
ALLOCATION OF DAMAGED ELECTRIC AND CYBER LINES

Depot	Damaged electric line	Damaged cyber line
Depot 1	3-4, 20-21, and 24-25	2-19, 4-5, and 23-24
Depot 2	11-12, 16-17, 27-28, and 31-32	7-8, 14-15, and 26-27

TABLE II
TRAVEL PATHS AND TIMETABLES OF DISPATCHABLE RESOURCES

Depot	Resource	Travel path [reaching time (min), leaving time (min)]
Depot 1	EMC1	24-25 [9, 81]→3-4 [95,167]→20-21 [175, 247]
	CMC	4-5 [18, 90]→2-19 [104, 176]
Depot 2	EMC2	31-32 [14, 86]→27-28 [101,173] → 11-12 [193, 265]→16-17 [283, 355]
	ECV	25-29 [24, 178]→14-15 [212, 360]

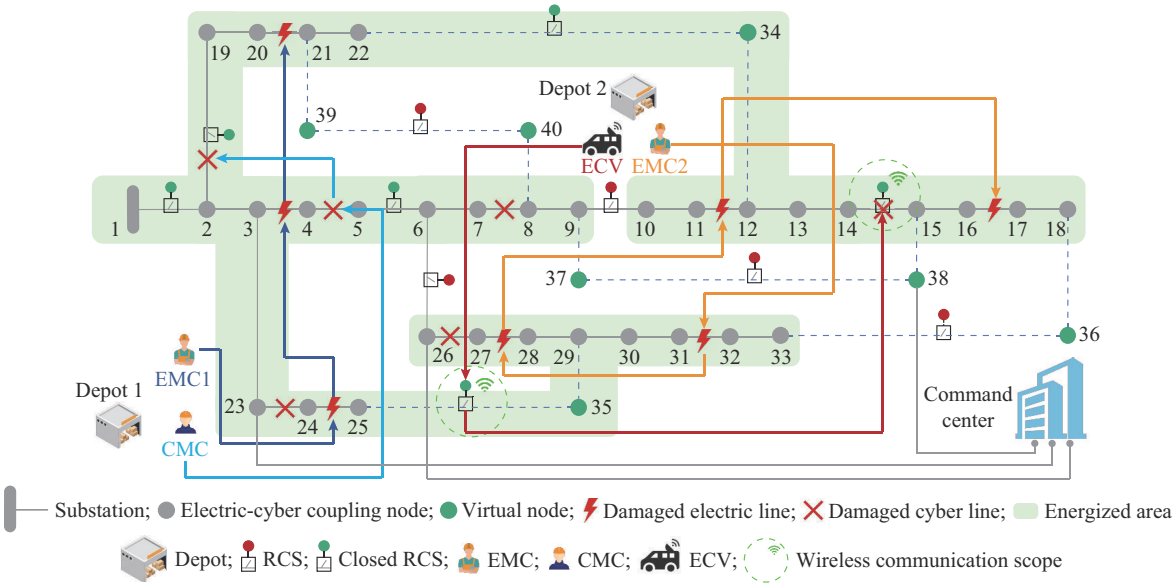

Fig. 5. Co-dispatching of three recovery resources and energized areas in IEEE 33-node test system.

The two EMCs repair all the damaged electric lines within 355 min. The damaged cyber lines 4-5 and 2-19 are repaired by a CMC to restore the cyber function of RCSs 5-6, 2-19, and 22-34. The other four damaged cyber lines are irrelevant to the recovery process after the decision and do not need to be repaired. The ECV travels to RCSs 25-35 and 14-15 using wireless communication to ensure that the switches could perform a timely close. Finally, six RCSs need to be closed to energize all the electric node blocks and ensure that the distribution system operates normally in a radial structure.

Furthermore, we also design five scenarios involving disasters and realistic settings for comparison to demonstrate the practicality and applicability of the proposed DSR framework. Scenario 1 is the benchmark failure scenario. In scenario 2, we simulate a realistic situation involving several electric line failures in the distribution system owing to the collapse of towers and tree barriers caused by extreme natural disasters [27]. In scenario 3, we simulate several man-made and targeted damages to cyber lines [28], which cause RCSs to be unresponsive for a long time during the recovery process. The available recovery resources in scenarios 1-3 are the same. In scenarios 4 and 5, recovery resources are added to evaluate their effects on DSR. The design and optimization results for the five scenarios are listed in Table III.

TABLE III
DESIGN AND OPTIMIZATION RESULTS FOR FIVE SCENARIOS

Scenario No.	Number of damaged lines		Available recovery resource	Total time to restore loads (min)	Total restored energy (kWh)	Computation time (s)
	Electric	Cyber				
1	7	6		360	9615.50	13.35
2	10	3	2 EMCs, 1 CMC, and 1 ECV	518	7980.17	22.98
3	3	10		181	15284.00	14.54
4	10	3	4 EMCs, 1 CMC, and 1 ECV	283	13884.67	25.87
5	3	10	2 EMCs, 3 CMCs, and 1 ECV	172	15624.25	48.27

The proposed DSR framework provides efficient recovery strategies for each scenario in a short time (less than 1 min). For scenarios 1-3, we can find that the total time needed to restore loads is proportional to the number of damaged electric lines because all of them need to be repaired. In contrast, increasing the number of damaged cyber lines may not necessarily increase the time required to restore the loads for two reasons.

1) The ECVs restore the cyber function of RCSs through wireless communications, thereby replacing part of the repair work of damaged cyber lines.

2) Only some damaged cyber lines can affect the DSR progress and need to be repaired.

Based on scenario 2, we add two EMCs to participate in electric recovery tasks in scenario 4. Compared with scenario 2, scenario 4 has a 45.4% reduction in the total time to restore loads and a 74% increase in the total restored energy. Similarly, compared with scenario 3, the total time to restore loads is reduced by 5.23% and the total restored energy is increased by 2.23% in scenario 5. Hence, we can conclude that the effect of DSR can be significantly enhanced in the scenario with a large number of damaged electric lines by increasing the number of EMCs. However, for scenarios with several damaged cyber lines, an increase in the number of CMCs may not result in a considerable improvement depending on the impact of damaged cyber lines on the DSR pro-

cess. For example, if most damaged cyber lines do not affect the normal operation of RCSs (i. e., the cyber lines do not need to be repaired), the supply of cyber recovery resources exceeds the demand, being useless to add more such resources. Hence, the appropriate number of resources for DSR should be selected in real-world scenarios.

B. IEEE 123-node Test System

The co-operation recovery strategies are also applied to the IEEE 123-node test system. The system voltage basis is 4.16 kV with a total load demand of 3490 kW [29]. In addition, we consider realistic parameter settings (e. g., repair time for damaged lines and closing time of RCSs) in this test system. The IEEE 123-node test system and corresponding TN modified for our case studies are shown in Figs. 6 and 7, respectively. The distribution system is equipped with 3 depots, 16 RCSs, 6 DGs, and 5 substations. For the failure scenario and recovery of resources, we assume 15 damaged electric lines and 13 damaged cyber lines, as shown in Fig. 6. Each depot is equipped with two EMCs and one CMC, and Depot 1 also contains one ECV.

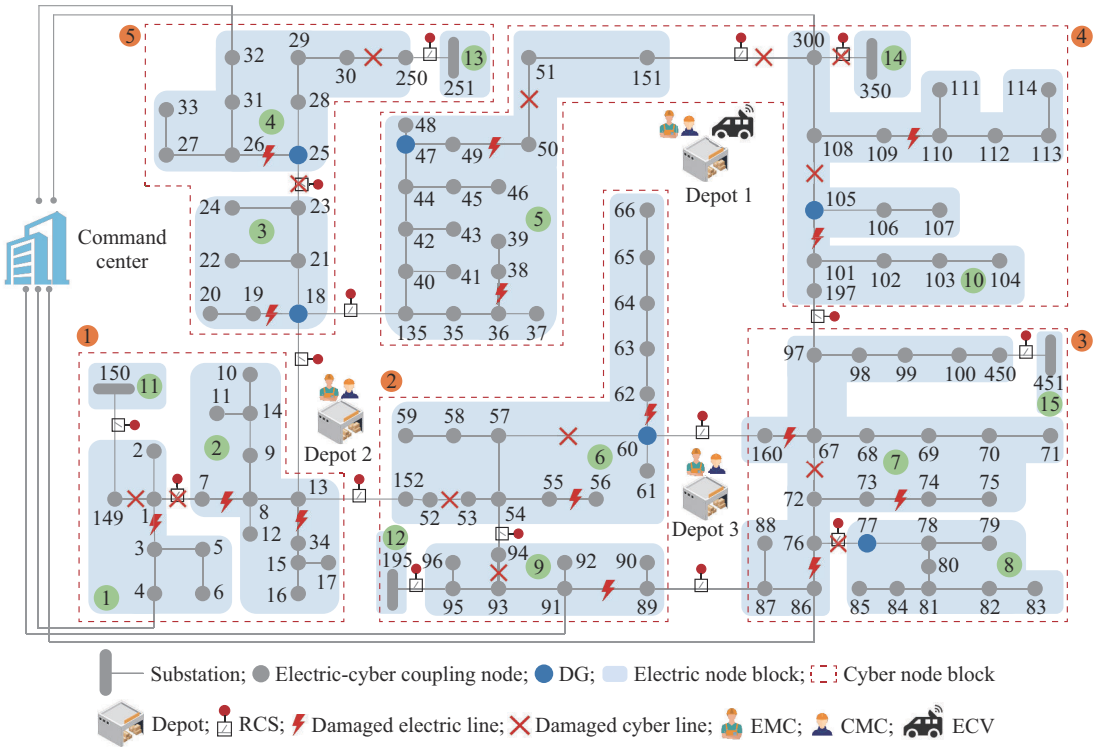

Fig. 6. Modified IEEE 123-node test system.

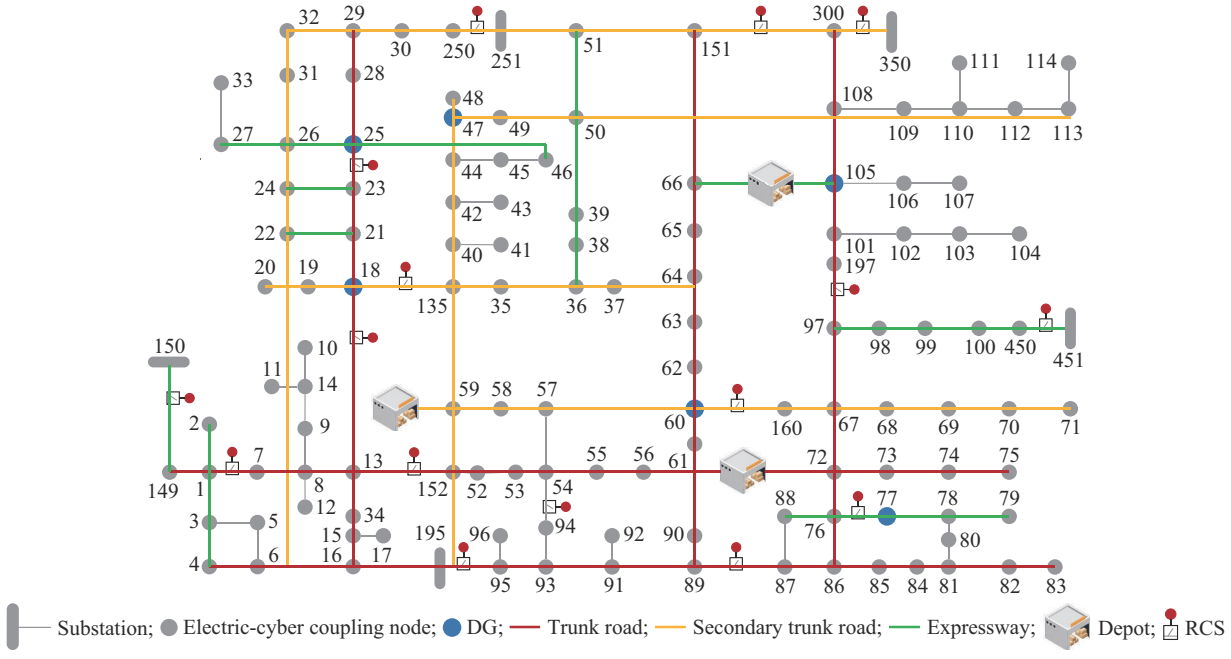

Fig. 7. TN topology for IEEE 123-node test system.

The repair time of the damaged electric lines for the EN and CN can be found in [29]. The repair time of damaged cyber lines and time required to close the RCSs $T_{a,b}^{\mathrm{RS}}$ are shown in Tables IV and V, respectively.

TABLE IV
REPAIR TIME OF DAMAGED CYBER LINE

Line	Time (min)	Line	Time (min)	Line	Time (min)
1-7	91	52-53	83	105-108	46
1-149	62	57-60	97	151-300	47
23-35	105	67-72	113	300-350	53
30-250	118	76-77	84		
50-51	50	93-94	58		

TABLE V
TIME REQUIRED TO CLOSE RCSS

Switch	Time (min)	Switch	Time (min)	Switch	Time (min)	Switch	Time (min)
1-7	2	23-25	5	87-89	4	151-300	3
13-18	3	54-94	3	95-195	1	250-251	1
13-152	3	60-160	3	97-197	5	300-350	1
18-135	2	76-77	2	149-150	1	450-451	1

The proposed co-optimization model is solved in 594 s. The co-dispatching paths of the EMCs in the IEEE 123-node test system are shown in Fig. 8, and those of the CMCs and ECV and energized areas in the IEEE 123-node test system are shown in Fig. 9. In Fig. 9, the energized areas are indicated by the blocks with different colors.

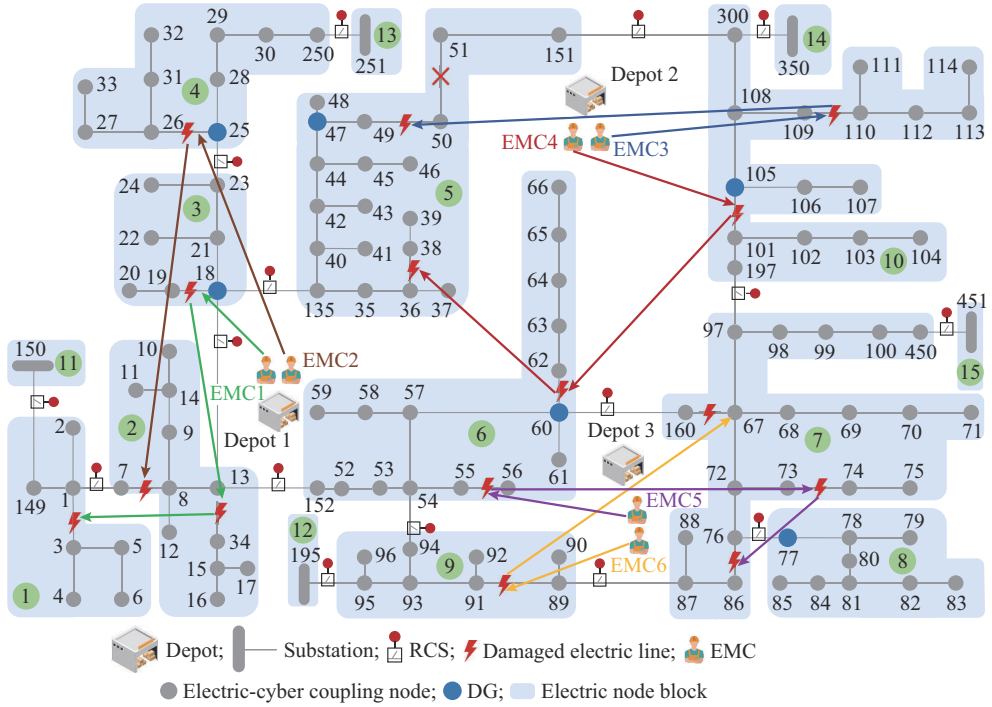

Fig. 8. Co-dispatching paths of six EMCs in IEEE 123-node test system.

To demonstrate the sequential DSR in detail, the timetables for the sequential recovery strategies are listed in Table VI. During the DSR, the collaborative recovery tasks include: ① repair of damaged electric and cyber lines; ② cyber function restoration for RCSs; ③ closing of RCSs; and ④ energization of node blocks.

In Table VI, *i-j** indicates that the cyber function of RCS *i-j* is restored by the ECV. The cyber functions of other RCSs are restored by repairing damaged cyber lines, including RCSs with intact cyber functions (e. g., RCS 95-195). Only during the ECV deployment and establishment of wireless communications for a period, the cyber function of RCS *i-j** is temporarily restored and the RCS could operate normally. Seven damaged cyber lines are repaired to restore the cyber function of the corresponding RCSs. The other six damaged cyber lines are irrelevant to DSR and do not need to be repaired. The operation constraints (31)-(36) of the distribution system only need to be checked at the energization time, $t_i^{\mathrm{R}} \in T^{\mathrm{R}}$, as described in Section II-C. Furthermore, t_i^{R} is equal to t_a^{DSRM}, as given by (27). Thus, we check the operation constraints at the energization time of the node blocks, including $t=0$ min, $t=110$ min (block 9), $t=122$ min (block 10), and the other eight energization time listed in Table VI.

The collaborative dispatching strategies for EMCs, CMCs, and ECVs are critical for accelerating the DSR. To better understand the coordination of the three dispatchable resources, Fig. 10 shows DSR steps for node blocks 7 and 8. First, the substation node block 15 is energized at $t=0$. Second, the damaged electric line 73-74 is repaired by EMC6 at $t=132$ min. Third, the damaged cyber line 67-72 is repaired by CMC3 at $t=225$ min, and the cyber function of RCS 450-451 is restored. In addition, the damaged electric lines 67-160 and 76-86 in node block 7 are repaired using EMC5 and EMC6 at $t=255$ min and 261 min, respectively.

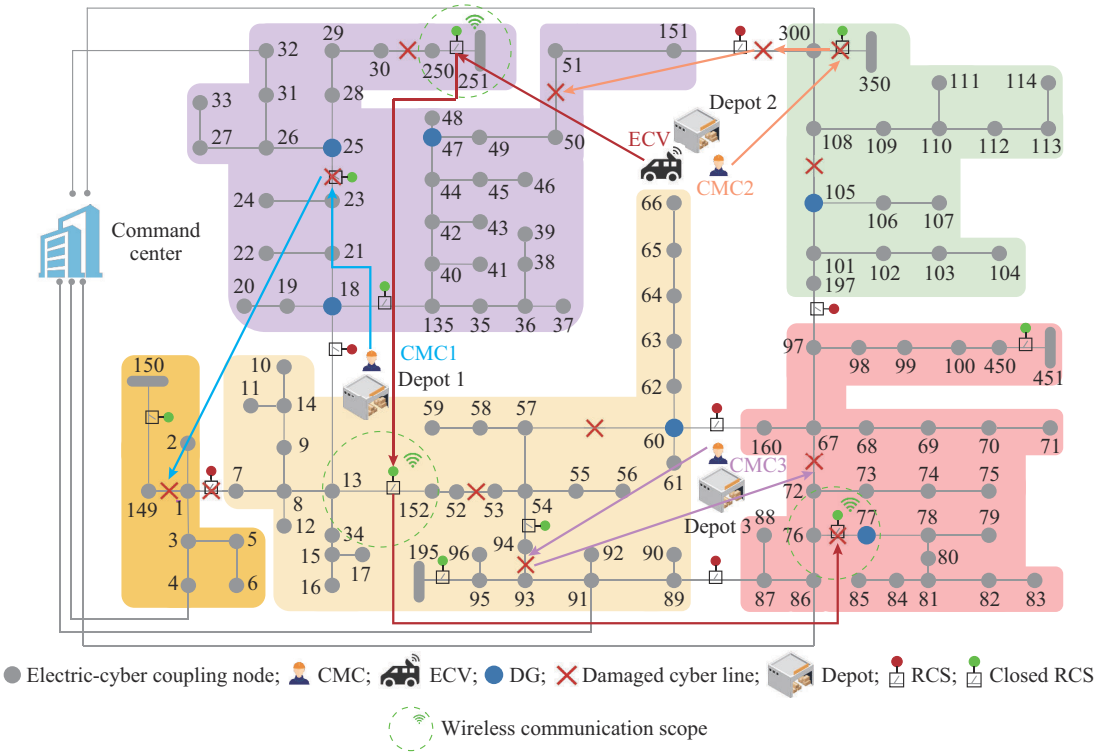

Fig. 9. Co-dispatching paths of three CMCs and one ECV and energized areas in IEEE 123-node test system.

TABLE VI
TIMETABLE OF SEQUENTIAL RECOVERY STRATEGIES

t (min)	Repaired line		RCS		Energized node block	Load restoration (kW)
	Electric	Cyber	Cyber function restoration	Closed		
0			95-195		11,12,13, 14,15	
40			250-251*			
57	101-105					
61	55-56					
71		300-350	300-350			
81		93-94	54-94			
103	18-19					
109	89-91					
110				95-195	9	160
121	109-110					
122				300-350	10	320
125	60-62					
126		23-25	23-25			
128				54-94	6	550
132	25-26 73-74					
133				250-251	4	200
138				23-25	3	160
141		50-51				
177			13-152*			
186			18-135			
196	13-34					
197		151-300				
216	7-8					
219				13-152	2	240
225		67-72	450-451			
226	49-50					
228		1-149	149-150			
251	36-38					
253				18-135	5	755
255	67-160		76-77*			
261	76-86					
262				450-451	7	705
267				76-77	8	240
310	1-3					
311				149-150	1	160

Simultaneously, the ECV reaches the RCS 76-77 at $t=255$ min, and the cyber function of RCS 76-77 is restored temporarily. Then, RCS 450-451 is closed at $t=262$ min to energize node block 7, and the loads (705 kW) are restored. Finally, RCS 76-77 is closed at $t=267$ min to energize node block 8, and the loads (240 kW) are restored.

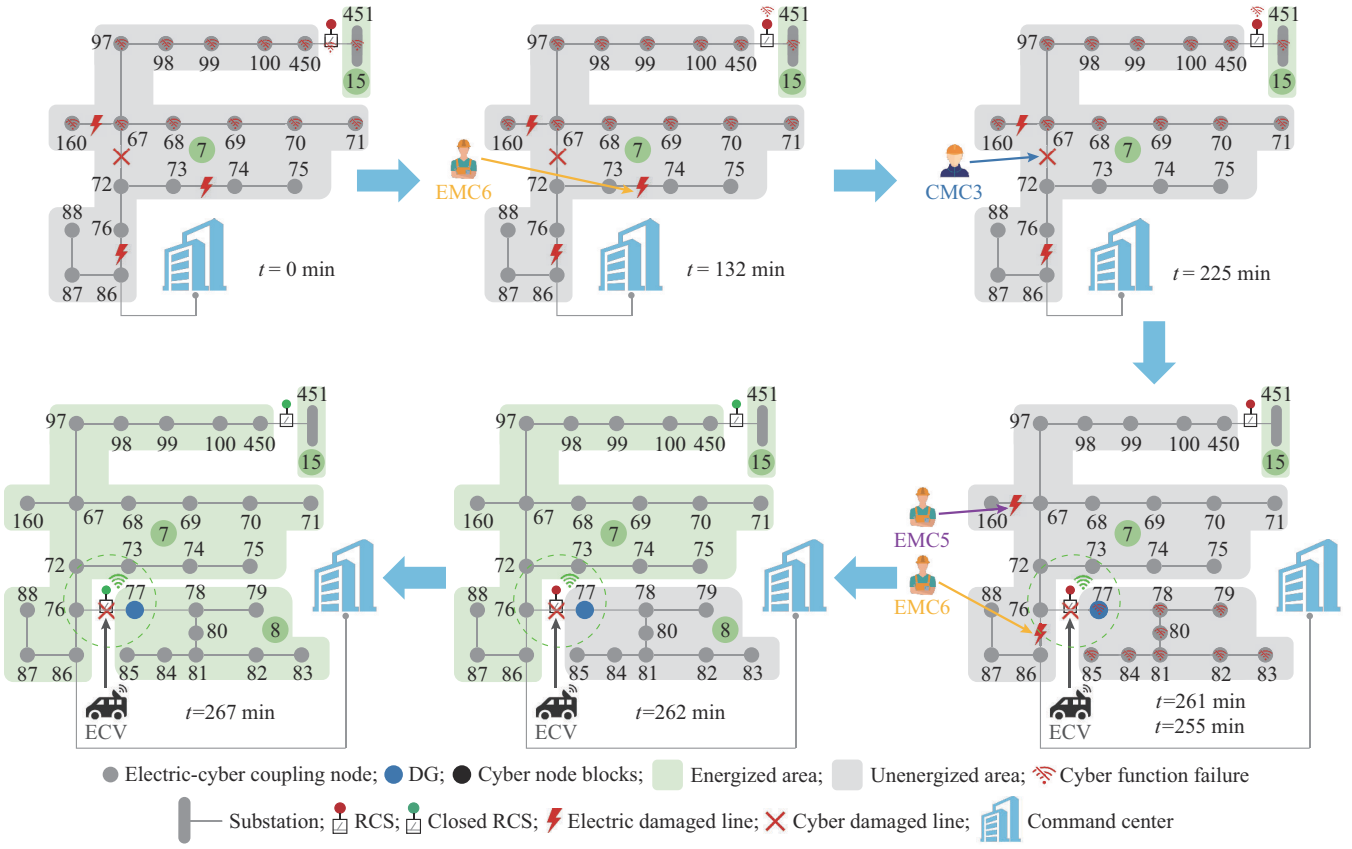

Fig. 10. DSR steps for electric node blocks 7 and 8.

To demonstrate the superiority of the proposed DSR framework, we design five cases and conduct a comprehensive comparison with existing DSR frameworks. The cooperation of CMCs and ECVs can accelerate the restoration of CNs and improve DSR efficiency, which is a prominent feature of the developed models. Thus, three state-of-the-art methods for DSR with CMCs or ECVs, and an advanced hierarchical optimization model are built for comparison with the proposed DSR framework.

Case 1: hierarchical optimization for DSR [29].

Case 2: only maintenance crews (excluding ECVs) follow an independent repair approach (IRA) [17] in DSR.

Case 3: similar to Case 2, only maintenance crews participate in the DSR, and the crews follow a joint repair approach (JRA) [17].

Case 4: optimization model for restoring CNs through ECV wireless communications only (excluding CMCs) in DSR [19].

Case 5: the proposed co-optimization models coordinate the dispatching of EMCs, CMCs, and ECVs to accelerate the load restoration in the distribution system described in the previous sections.

The above five cases are conducted for DSR considering the design and parameters of the IEEE 123-node test system, as described in Section IV-B. The settings of the five cases are listed in Table VII.

TABLE VII
SETTINGS OF FIVE CASES

Case	Rule	Model	Dispatchable resource
1	EMCs in EN and CMCs, ECV in CN	A hierarchical optimization model [29]	6 EMCs, 3 CMCs, and 1 ECV
2	Only maintenance crews for DSR	IRA [17]	6 EMCs and 4 CMCs
3	Only maintenance crews for DSR	JRA [17]	10 maintenance crews
4	EMCs in EN and only ECV in CN	An integrated DSR framework [19]	6 EMCs and 4 ECVs
5	EMCs in EN and CMCs, ECV in CN	Proposed	6 EMCs, 3 CMCs, and 1 ECV

The comparison results of the restored power and energy of loads for the five cases are shown in Fig. 11.

For Case 1, it takes the longest time (383 min) to restore all loads and has the lowest restored energy of loads (6635.67 kWh). Case 1 emphasizes repairing damaged lines in the shortest time when dispatching EMCs and CMCs. However, Case 1 might show uncoordinated repair of damaged electric and cyber lines by maintenance crews. For example, damaged electric lines in the area could be restored while the cyber function of RCS is not restored. This will

prevent RCSs from closing and prevent loads from being restored for a long time, thus being inefficient. As shown in Fig. 11, the RCSs fail to close within $t=122-268$ min and $t=272-343$ min owing to uncoordinated repair strategies.

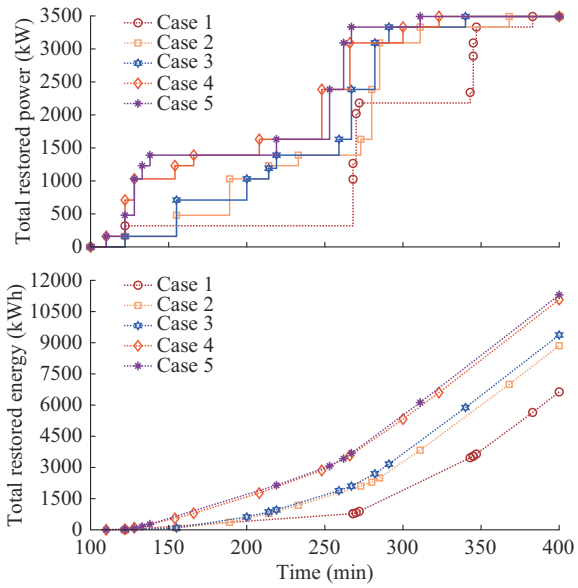

Fig. 11. Restored power and energy in five cases.

Both Cases 2 and 3 consider that only maintenance crews (excluding ECVs) participate in DSR. Although the number of maintenance crews is the same in Cases 2 and 3, 10 maintenance crews in Case 3 could repair both the damaged electric and cyber lines. Six EMCs repair the EN and four CMCs repair the CN, which is fixed in Case 2. The repair strategy in Case 3 provides better dispatching flexibility than that in Case 2. In other words, Case 3 can allocate different numbers of maintenance crews to repair damaged electric and cyber lines in different periods, substantially improving the recovery efficiency for both networks. As shown in Fig. 11, Case 3 could restore all the loads within 340 min, being 28 min earlier than Case 2. Moreover, the total restored energy for Case 3 is 9373.25 kWh, being 515.17 kWh higher than that for Case 2.

Both Cases 4 and 5 coordinate the maintenance crews and ECVs to restore loads in DSR. However, only ECVs participate in restoring the cyber function of the RCSs in Case 4, possibly providing a difference in the performance of ECVs compared with CMCs in terms of cyber restoration. In particular, when damaged electric lines in an area are repaired, the corresponding RCS is required to energize and restore the loads in that area. However, the cyber function of the RCSs might be lost, impeding them to be closed. There are two conditions (C1 and C2) for CMCs and ECVs to restore the cyber function of RCSs.

C1: the time required to restore the cyber function of RCS by repairing damaged cyber lines is much less than that required to complete the repair of damaged electric lines in an area. CMCs can restore the cyber function of an RCS before it must be closed. However, the ECV must remain in place until all damaged electric lines are repaired. The recovery efficiency of the CMC is higher in C1.

C2: the time required to restore the cyber function of RCS by repairing damaged cyber lines is much longer than that for completing the repair of damaged electric lines in an area. Once the damaged electric lines in the area are repaired, the ECV can immediately provide wireless communications to restore the cyber function of the RCS. However, CMCs may be still repairing damaged cyber lines, preventing the RCS from closing for a long time. The recovery efficiency of the ECV is higher in C2.

Both C1 and C2 may occur in real-world situations, and either CMCs or ECVs should be selected to restore the cyber function of RCSs according to different situations. Therefore, the collaborative recovery in Case 5 is better than that in Case 4. As shown in Fig. 11, all loads are restored within 311 min in Case 5, being 12 min earlier than that in Case 4. In addition, the total restored energy in Case 5 is 11302.58 kWh, being 225.75 kWh higher than that in Case 4. As ECVs are scarce resources, it would be unreasonable to allocate several ECVs for DSR. The proposed co-optimization of CMCs and ECVs for cyber function restoration seems valuable and applicable in practice.

Figure 11 also shows that the performance of global optimization model (Cases 2-5) is much better than that of the hierarchical optimization model (Case 1) for DSR. The total restored energy obtained from the global optimization model is 51.9% higher on average than that from hierarchical optimization model. In addition, using ECVs as cyber recovery resources for RCSs can considerably improve the efficiency of load restoration. Compared with Cases 2 and 3 in which only CMCs are involved in CN restoration, the total restored energy in Cases 4 and 5 increase by 22.9% on average.

V. Conclusion

To accelerate DSR after extreme events, we propose a co-optimization model for the dispatch of EMCs, CMCs, and ECVs while considering the coupling of ENs, CNs, and TNs. We introduce specific optimization models and response solution methods to reduce the computational complexity. The effectiveness and superiority of the proposed DSR framework are verified using modified IEEE 33-node and 123-node test systems. The numerical results demonstrate that the proposed DSR framework can reduce the load recovery time and increase the total restored energy in DSR. Additionally, the proposed DSR framework exhibits good applicability and practicality by considering real-world scenarios and settings.

To conduct more comprehensive research, we can mention the following limitations and directions of future work.

1) As prior misjudgments and secondary failures may exist in real-world scenarios, maintenance crews may not carry sufficient supplies for repair tasks and may need to return to the depots for resupplying. Hence, the resource constraints of the corresponding proposed models should be further refined.

2) DSR data often contain uncertainties and dynamic factors such as load demands, repair time of damaged components, and travel time of dispatchable resources. Such uncertainties should be investigated in future studies.

3) Other technical constraints and considerations for DSR can be added to the proposed DSR framework, such as cold load pickup, renewable energy sources, unbalanced distribution systems, and robust and stochastic optimization techniques.

REFERENCES

[1] Y. Wang and B. Pal, "Destabilizing attack and robust defense for inverter-based microgrids by adversarial deep reinforcement learning," *IEEE Transactions on Smart Grid*, vol. 14, no. 6, pp. 4839-4850, Nov. 2023.

[2] L. Xu, Q. Guo, Y. Sheng *et al*., "On the resilience of modern power systems: A comprehensive review from the cyber-physical perspective," *Renewable and Sustainable Energy Reviews*, vol. 152, p.111642, Dec. 2021.

[3] X. Liu, Q. Wu, J. Sun *et al*., "Research on self-healing technology for faults of intelligent distribution network communication system," in *Proceeding of 2019 IEEE 3rd Information Technology, Networking, Electronic and Automation Control Conference (ITNEC)*, Chengdu, China, Mar. 2019, pp. 1404-1408.

[4] D. Xie, Y. Xu, and C. Zhang, "Robust service restoration of distribution systems towards coordinated parallel network reconstruction and cold load pick-up," *International Journal of Electrical Power & Energy Systems*, vol. 152, p. 109187, Oct. 2023.

[5] H. Sekhavatmanesh and R. Cherkaoui, "A multi-step reconfiguration model for active distribution network restoration integrating DG start-up sequences," *IEEE Transactions on Sustainable Energy*, vol. 11, no. 4, pp. 2879-2888, Oct. 2020.

[6] F. Shen, Q. Wu, J. Zhao *et al*., "Distributed risk-limiting load restoration in unbalanced distribution systems with networked microgrids," *IEEE Transactions on Smart Grid*, vol. 11, no. 6, pp. 4574-4586, Nov. 2020.

[7] C. Wang, J. Sun, M. Huang *et al*., "Two-stage optimization for active distribution systems based on operating ranges of soft open points and energy storage system," *Journal of Modern Power Systems and Clean Energy*, vol. 10, no. 1, pp. 66-79, Jan. 2023.

[8] Q. Sun, Z. Wu, W. Gu *et al*., "Multi-stage co-planning model for power distribution system and hydrogen energy system under uncertainties," *Journal of Modern Power Systems and Clean Energy*, vol. 10, no. 1, pp. 80-93, Jan. 2023.

[9] C Lin, C Chen, F Liu *et al*., "Dynamic MGs-based load restoration for resilient urban power distribution systems considering intermittent RESs and droop control," *International Journal of Electrical Power & Energy Systems*, vol. 140, p. 107975, Sept. 2022.

[10] Q. Zhang, Z. Ma, Y. Zhu *et al*., "A two-level simulation-assisted sequential distribution system restoration model with frequency dynamics constraints," *IEEE Transactions on Smart Grid*, vol. 12, no. 5, pp. 3835-3846, Jun. 2021.

[11] Q. Zhang, Z. Wang, S. Ma *et al*., "Stochastic pre-event preparation for enhancing the resilience of distribution systems," *Renewable and Sustainable Energy Reviews*, vol. 152, p. 111636, Dec. 2021.

[12] Z. Ye, C. Chen, B. Chen *et al*., "Resilient service restoration for unbalanced distribution systems with distributed energy resources by leveraging mobile generators," *IEEE Transactions on Industrial Informatics*, vol. 17, no. 2, pp. 1386-1396, Feb. 2021.

[13] S. Paul, F. Ding, K. Utkarsh *et al*., "On vulnerability and resilience of cyber-physical power systems: a review," *IEEE Systems Journal*, vol. 16, no. 2, pp. 2367-2378, Jun. 2022.

[14] M. K. Hasan, A. K. M. A. Habib, Z. Shukur *et al*., "Review on cyber-physical and cyber-security system in smart grid: standards, protocols, constraints, and recommendations," *Journal of Network and Computer Applications*, vol. 209, p. 103540, Jan. 2023.

[15] B. Ti, G. Li, M. Zhou *et al*., "Resilience assessment and improvement for cyber-physical power systems under typhoon disasters," *IEEE Transactions on Smart Grid*, vol. 13, no. 1, pp. 783-794, Jan. 2022.

[16] J. Lu, X. Xie, X. Zhou *et al*., "Research on power-communication coordination recovery strategy based on grid dividing after extreme disasters," in *Proceedings of IOP Conference Series: Earth and Environmental Science*, Xiamen, China, Nov. 2020, p. 012038.

[17] M. Tian, Z. Dong, L. Gong *et al*., "Coordinated repair crew dispatch problem for cyber-physical distribution system," *IEEE Transactions on Smart Grid*, vol. 14, no. 3, pp. 2288-2300, May 2023.

[18] X. Sun, J. Chen, H. Zhao *et al*., "Sequential disaster recovery strategy for resilient distribution network based on cyber-physical collaborative optimization," *IEEE Transactions on Smart Grid*, vol. 14, no. 2, pp. 1173-1187, Mar. 2023.

[19] Z. Ye, C. Chen, R. Liu *et al*., "Boost distribution system restoration with emergency communication vehicles considering cyber-physical interdependence," *IEEE Transactions on Smart Grid*, vol. 14, no. 2, pp. 1262-1275, Mar. 2023.

[20] H. Zhang, C. Chen, S. Lei *et al*., "Resilient distribution system restoration with communication recovery by drone small cells," *IEEE Transactions on Smart Grid*, vol. 14, no. 2, pp. 1325-1328, Mar. 2023.

[21] Z. Li, W. Tang, X. Lian *et al*., "A resilience-oriented two-stage recovery method for power distribution system considering transportation network," *International Journal of Electrical Power & Energy Systems*, vol. 135, p. 107497, Feb. 2022.

[22] X. Jiang, J. Chen, M. Chen *et al*., "Multi-stage dynamic post-disaster recovery strategy for distribution networks considering integrated energy and transportation networks," *CSEE Journal of Power and Energy Systems*, vol. 7, no. 2, pp. 408-420, Mar. 2021.

[23] B. Li, Y. Chen, W. Wei *et al*., "Resilient restoration of distribution systems in coordination with electric bus scheduling," *IEEE Transactions on Smart Grid*, vol. 12, no. 4, pp. 3314-3325, Jul. 2021.

[24] B. Zhang, L. Zhang, W. Tang *et al*., "A coordinated restoration method of electric buses and network reconfiguration in distribution systems under extreme events," *CSEE Journal of Power and Energy Systems*, doi: 10.17775/CSEEJPES.2020.04320

[25] H. Pan, H. Lian, C. Na *et al*., "Modeling and vulnerability analysis of cyber-physical power systems based on community theory," *IEEE Systems Journal*, vol. 14, no. 3, pp. 3938-3948, Sept. 2020.

[26] S. H. Dolatabadi, M. Ghorbanian, P. Siano *et al*., "An enhanced IEEE 33 bus benchmark test system for distribution system studies," *IEEE Transactions on Power Systems*, vol. 36, no. 3, pp. 2565-2572, May 2021.

[27] S. McDonell. (2016, Sept.). Typhoon Meranti mop up continues in southern China. [Online]. Available: https://www. bbc. com/news/av/world-asia-37372785

[28] E-ISAC and SANS. (2016, Mar.). Analysis of the cyber attack on the Ukrainian power grid: defense use case. [Online]. Available: https://ics.sans.org/duc5

[29] G. Zhang, F. Zhang, X. Zhang *et al*., "Sequential disaster recovery model for distribution systems with co-optimization of maintenance and restoration crew dispatch," *IEEE Transactions on Smart Grid*, vol. 11, no. 6, pp. 4700-4713, Nov. 2020.

Zhengze Wei received the B. S. degree from Fuzhou University, Fuzhou, China, in 2021. He is currently working toward the M. S. degree with the School of Electrical Engineering, Chongqing University, Chongqing, China. His current research interests include distribution system restoration and operation optimization in power system.

Kaigui Xie received the Ph. D. degree in power system and its automation from Chongqing University, Chongqing, China, in 2001. He is a currently a Full Professor with the School of Electrical Engineering, Chongqing University. His research interests include power system reliability, planning, and analysis.

Bo Hu received the received the Ph.D. degree in electrical engineering from Chongqing University, Chongqing, China, in 2010. He is currently working as a Full Professor with the School of Electrical Engineering. His research interests include power system reliability and parallel computing techniques in power systems.

Yu Wang received the B. Eng. degree in electrical engineering and automation from Wuhan University, Wuhan, China in 2011, and the M.Sc. and Ph.D. degrees in Power Engineering from Nanyang Technological University, Singapore, in 2012 and 2017, respectively. Currently, he is a Professor at the School of Electrical Engineering, Chongqing University, Chongqing, China. He was a Marie Skłodowska-Curie Individual Fellow at Control & Power Group, Imperial College London, London, UK. His research interests include microgrid control and stability, power system operation and control, and cyber-physical systems.

Changzheng Shao received the B. S. degree in electrical engineering from Shandong University, Jinan, China, and the Ph. D. degree in electrical engineering from Zhejiang University, Hangzhou, China, in 2015 and 2020, respectively. He is currently an Assistant Professor with Chongqing University, Chongqing, China. His research interests include operation optimization

and reliability evaluation of integrated energy system.

Pierluigi Siano received the M.Sc. degree in electronic engineering and the Ph.D. degree in information and electrical engineering from the University of Salerno, Salerno, Italy, in 2001 and 2006, respectively. He is a Professor and Scientific Director of the Smart Grids and Smart Cities Laboratory with the Department of Management and Innovation Systems, University of Salerno. His research interests include demand response, energy management, integration of distributed energy resources in smart grids, electricity markets, and planning and management of power systems.

Jun Zhong received the Ph.D. degree in electrical engineering from Chongqing University, Chongqing, China, in 2017. He is currently working as a Senior Engineer in Shenzhen Power Supply Co., Ltd., China Southern Power Grid, Shenzhen, China. His main research interests include asset management and resilience planning and analysis in distribution system.